WELDING RESEARCH

SUPPLEMENT TO THE *WELDING JOURNAL,* JANUARY 2003
Sponsored by the American Welding Society and the Welding Research Council

Friction Stir Welding Studies on Mild Steel

Process results, microstructures, and mechanical properties are reported

BY T. J. LIENERT, W. L. STELLWAG, JR., B. B. GRIMMETT, AND R. W. WARKE

ABSTRACT. The objective of this work was to demonstrate the feasibility of friction stir welding (FSW) for joining of mild steel. Defect-free welds were produced on 0.25-in. plates (6.3 mm) of hot-rolled AISI 1018 mild steel at travel speeds ranging from 1 to 4 in./min (0.42 to 1.68 mm/s) using molybdenum-based and tungsten-based alloy tools. Results for welds made at 1 in./min are reported here. Axial tool loads measured during FSW were approximately 4200 lbf (18.7 kN), while measured torques were in the range of 500 in.-lb (55 N•m). Peak surface temperatures close to 1000°C (1832°F) were measured on the workpiece and tool during welding using thermocouples and an infrared camera system. Comparisons before and after welding combining both metallographic and metrology techniques suggest changes in tool dimensions stem from both rubbing wear and deformation of the tool. The greatest changes in tool dimensions occurred during the initial plunging stage. Microstructures of the welds were examined using optical and scanning electron microscopy. The weld region displayed several microstructurally distinct regions. Extrapolation of measured temperatures and microstructural evidence suggest peak temperatures of the stir zone exceeded 1100°C (2012°F) and likely surpassed 1200°C (2192°F). Transverse tensile properties of the welds were evaluated at room temperature. Welded samples failed in regions corresponding to the base metal and demonstrated yield and ultimate tensile strengths comparable to those of the base metal. Welded samples passed bend tests to ~15% strain in the outer fiber. The results have demonstrated the feasibility of FSW of steel with acceptable tensile properties. Based on these results, FSW of transformation-hardenable steels, HSLA steels, and stainless steels appears feasible.

T. J. LIENERT is a Technical Staff Member at Los Alamos National Laboratory, Los Alamos, N.Mex. W. L. STELLWAG, JR., and B. B. GRIMMETT are Application Engineers with Edison Welding Institute, Columbus, Ohio. R. W. WARKE is an Engineer with Southwest Research Institute, San Antonio, Tex.

Introduction

Friction stir welding (FSW) is a relatively new joining process that is presently attracting considerable interest (Ref. 1). The FSW process was developed at TWI in 1991. Figure 1 shows a schematic of the FSW process for joining of two plates in a square groove configuration (Ref. 2). The process is solid-state in nature and relies on localized forging of the weld region to produce the joint. The plates comprising the workpiece are held in compression and are rigidly fixtured to the machine bed during welding. Friction stir welding uses a nonconsumable, rotating tool that is cylindrical in shape with a cylindrical pin of smaller diameter extending from the tool shoulder. Important process parameters include the tool rpm and travel speed, as well as the tool dimensions and the downward force on the tool.

Initially, the rotating tool is plunged into the joint until the shoulder contacts the top surface of the workpiece. Heating is caused by rubbing of the tool faces against the workpiece (Refs. 3, 4) and by visco-plastic dissipation of mechanical energy (Refs. 5, 6) at high strain rates (Ref. 7) developed through interactions with the tool. During welding, the material along the joint is heated to a softened condition, transferred around the periphery of the tool, and subsequently recoalesced along the back surface of the pin to produce the weld.

KEY WORDS

Friction Stir Welding
Mild Steel
Torque
Tool Wear
Axial Load
Microstructures
Mechanical Properties
Peak Temperatures

Friction stir welding of Al alloys is relatively well established. To date, friction stir welds have been successfully produced on many of the important commercial Al alloys including the 1xxx (Ref. 8), 2xxx (Refs. 9–11), 5xxx (Refs. 12, 13), 6xxx (Refs. 12–17), and 7xxx (Refs. 18–20) families of alloys, as well as Al-Cu-Li alloys (Refs. 21, 22). Friction stir welding of Al alloys has several advantages over fusion welding processes. First, problems with solidification cracking, liquation cracking, and porosity are eliminated due to the solid-state nature of the process. Consequently, FSW permits joining of most, if not all, Al alloys, including those considered unweldable with fusion welding processes (Ref. 23). Moreover, friction stir welds often exhibit improved mechanical properties relative to those of fusion welds on the same material (Refs. 14, 15, 21). Finally, residual stresses and distortion in friction stir welds are typically lower than those of fusion welds (Ref. 24). The improvements in mechanical properties, residual stresses, and distortion relative to fusion welding are thought to stem from the lower heat input inherent with FSW. However, no heat input data has been reported for FSW.

Friction stir welds on Al alloys display several microstructurally distinct regions including the stir zone or nugget (along the weld centerline), the heat-and-deformation-affected zone (HDAZ) or thermomechanically affected zone (TMAZ) (surrounding the stir zone), and a true heat-affected zone (HAZ) (encompassing the HDAZ) (Refs. 11, 13, 15, 16, 18, 19). Microstructural evolution in the different regions of the weld zone is

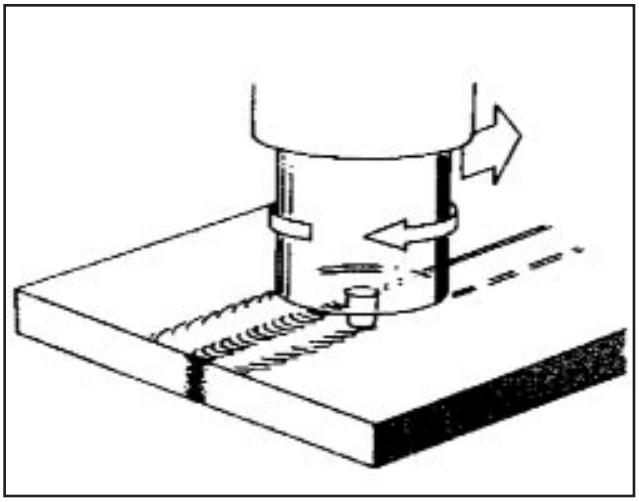

Fig. 1 — Schematic representation of the FSW process for butt joint welding. The FSW tool is rotated and traversed along the joint to produce the weld (Ref. 2).

closely linked with the local thermomechanical cycle experienced during joining. Important parameters of the thermomechanical cycle that control microstructural evolution are the total strain, the strain rate, and the temperature (Ref. 25).

The thermomechanical cycle experienced by the material in the stir zone of Al alloys essentially involves hot working. The stir zone is subjected to the greatest strain and strain rates (Ref. 7), as well as the highest temperatures (Refs. 4, 19). This combination of parameters apparently results in dissolution of strengthening precipitates as well as continuous dynamic recrystallization (Refs. 11, 15, 19, 22) in friction stir welds on Al alloys, although some debate exists regarding the latter subject. Material of the HDAZ of Al alloys experiences lower temperatures in addition to lower strains and strain rates relative to the stir zone (Ref. 15). The HDAZ appears to undergo dissolution and/or coarsening of strengthening precipitates but no dynamic recrystallization. As in fusion welds, the true HAZ of friction stir welds on Al alloys is subjected to a thermal cycle that apparently causes coarsening of the strengthening precipitates but very little strain (Refs. 10, 11, 15–18).

While most of the FSW efforts to date have involved joining of Al alloys, there is considerable interest in extending the technology to other materials, including steels (Refs. 26–28). Friction stir welding appears to offer several advantages over arc welding of steels. The lower apparent energy inputs of FSW are expected to minimize grain growth in the HAZ and limit distortion and residual stress in steels. Minimization of distortion and residual stress is extremely important in welding of thick-section material, such as in the shipbuilding and heavy manufacturing industries. Replacement of arc welding with FSW will also likely eliminate welding fumes, especially those containing hexavalent Cr (Cr^{VI}), to allow compliance with anticipated OSHA standards announced recently (Ref. 29). Additionally, problems with hydrogen cracking in steels are eliminated since FSW is a solid-state process. Taken together, these advantages make FSW attractive for joining of steel in many applications.

This work was undertaken as part of a larger effort to understand FSW of several types of steels including mild steels, transformation-hardenable steels, HSLA steels, and stainless steels. Mild steel was chosen for the initial part of the study reported here. The major objectives of this work were to demonstrate the feasibility of FSW for joining of mild steel by characterizing the process, microstructures, and mechanical properties of friction stir welds on mild steel.

Experimental Procedures

Friction stir welds were produced on plates of hot-rolled AISI 1018 steel (0.25 in. or 6.35 mm thick) with the welding direction parallel to the rolling direction of the plates. The composition of this heat of 1018 steel was determined using a combination of LECO and X-ray fluorescence methods and is given in Table 1. Welds were made in the square groove butt-joint configuration on samples typically 8 in. (20.3 cm) in length and 4 in. (10.1 cm) in width. The shoulder diameter of the tool was 0.75 in. (19 mm), and the pin length was approximately 0.245 in. (6.22 mm). Tool materials included both molybdenum- and tungsten-based alloys. Friction stir welds were produced at travel speeds ranging from 1 to 4 in./min (0.42 to 1.68 mm/s), and the tools were rotated at 450 to 650 revolutions per minute (rpm) during welding. The tool and weld area were protected from oxidation by inert gas shielding in a clear Plexiglass box. Further details of tool design and FSW processing are presented elsewhere (Ref. 1).

Deformation and wear of the tool are important issues for FSW of steels since changes in tool dimensions can affect weld quality. However, these changes are not easily quantified. Weight change of the tool is not necessarily a good indicator of wear since both loss of tool material and pickup of workpiece material on the tool can occur simultaneously. Similarly, measurement of different tool dimensions can be complicated by simultaneous pickup of workpiece material by the tool and by deformation of the pin. Tool deformation and wear were assessed in this study by comparing critical tool dimensions for a given tool before and after each weld using an optical comparator. Separate measurements were also made before and after plunge tests. The weld tests included a plunging period and a welding period, while the plunge test involved only plunging, followed by immediate retraction. These procedures were repeated several times to determine average changes in tool dimensions for plunging and welding stages.

Table 1 — Measured Composition of 1018 Mild Steel (all wt-%)

% C	% Mn	% P	% S	% Si
0.18	0.82	0.011	0.006	<0.01

Knowledge of tool load, torque, and temperature during FSW is very useful from the standpoint of process development. Axial loads and torques on the tool were determined during each weld using a calibrated strain gauge set attached to the tool holder. Tools were modified to internally accept a thermocouple near the pin. Thermocouples were also attached to the outer circumference of the tool at various distances above the shoulder. The strain gauges and thermocouples were hard wired to modules attached to the machine spindle. Data from the load, torque, and temperature modules were transmitted during welding from the rotating spindle via an antenna system to a data acquisition system and then downloaded to a personal computer. The torque and load instrumentation was calibrated prior to welding using load cells. After welding, features on each weld sample were spatially and temporally correlated with the different signals. The dominant frequencies associated with the load and torque traces were determined using a Fast-Fourier Transform (FFT) program to gain possible process insight.

Determination of workpiece temperature distribution is not trivial. Thermocouples placed to intersect the stir zone region often are crushed or displaced by the deforming material of the stir zone before reaching peak temperatures, thereby introducing uncertainties in measurement. In addition, thermocouples attached to the top surface of the workpiece close to the edge of the stir zone are often severed by extrusion of the flashing from under the

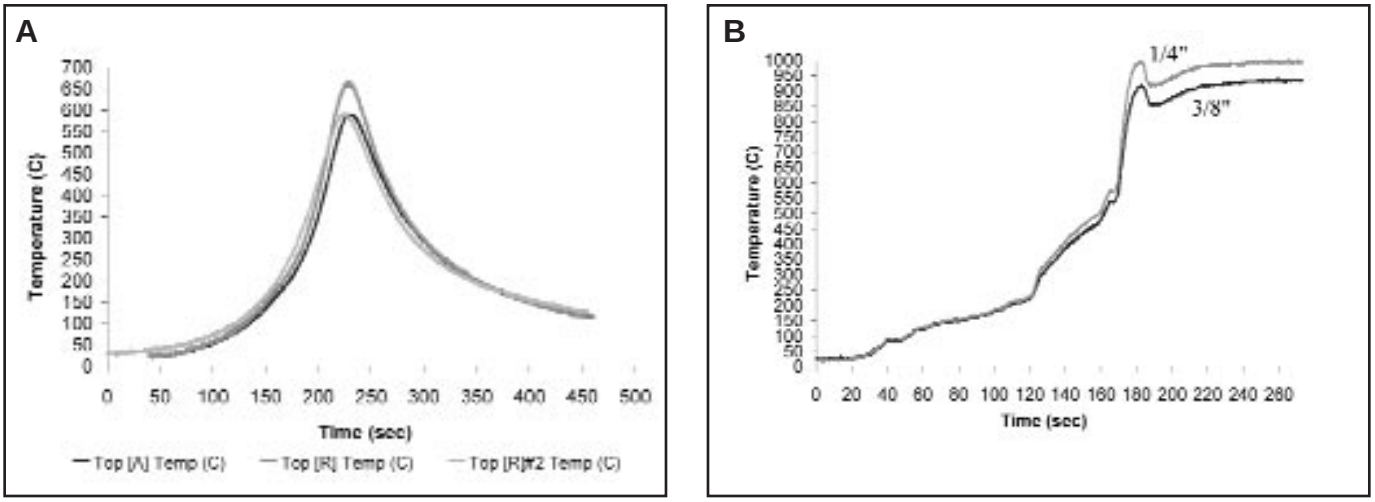

Fig. 2 — A — Temperature cycles for thermocouples located at ~0.125 in. (3.2 mm) from the edge of the stir zone on the top surface of the 1018 steel workpiece; B — temperature cycles for thermocouples located at 0.25 and 0.38 in. (6.35 and 9.65 mm) above the tool shoulder.

tool shoulder before reaching peak temperatures. To circumvent this problem, thermocouples were attached to the workpiece in shallow grooves at several locations on the top and bottom surfaces in this study. This method allowed the flashing to slide over the top of the groove without disturbing the thermocouples.

Tool and workpiece temperatures were also monitored using an Agema 550 Tracer Plus Elite Infrared System from FLIR systems. The camera uses a focal plane array detector with a spectral range of 3.6 to 5.0 microns. The array consists of a 320 x 240 platinum-silicon (PtSi) detector yielding a spatial resolution of 76,800 pixels. The camera temperature range is –20°C (–4°F) to 2000°C (3632°F), with a measurement accuracy of ±2% or 2°C of the temperature range. The field of view for this camera is 20 deg x 15 deg with the standard lens. The camera produces images with 256 color levels with a user-selected palette. Accurate temperature measurement with this system requires user input of correct emissivity values. For each weld, the emissivity was calibrated against known temperatures from the thermocouples placed on the tool.

Metallographic samples were produced from welds made at 1 in./min using standard procedures and etched with a 2% nital solution. Etched samples were examined using optical microscopy (OM) with differential interference contrast (DIC) and scanning electron microscopy (SEM) with X-ray energy-dispersive spectroscopy (EDS). Weld microstructures were classified according to a scheme developed by the International Institute for Welding (IIW) (Ref. 30). Vickers microhardness traverses (1-mm increments) were produced across the weld regions using a 500-g load and a 15-s dwell time. Mechanical properties of samples from welds made at 1 in./min were evaluated by transverse tensile testing of subscale specimens at room temperature according to ASTM E8 (Ref. 31). Tensile samples were prepared by milling of the top and bottom surfaces to remove flashing and other surface irregularities. Face and root bend tests were also performed on machined specimens of the welded samples (0.25 x 1 x 6 in. or 6.35 x 25.4 x 152.4 mm) using a die block with a 0.75-in. (19-mm) radius.

Results

In this study, friction stir welds were produced on 1018 steel at travel speeds ranging from 1 to 4 in./min (0.42 to 1.68 mm/s). However, results reported here pertain mainly to welds made at 1 in./min travel speed.

Process Characterization

Load, torque, and temperature data were recorded as functions of time for several defect-free welds. Conversion of the different data sets to plots as a function of distance was accomplished by multiplying by the weld travel speed.

The tool and the flashing around the tool glowed a reddish-orange color during welding suggesting peak temperatures of at least 1100°C (2012°F). Thermal cycles recorded from the workpiece and the tool are presented in Figs. 2A and B, respectively. Thermocouples placed approximately 0.125 in. from the edge of the stir zone at the top of the plate recorded peak temperatures between 590°C (1094°F) and 665°C (1229°F) — Fig. 2A. Observe that the thermal cycles were relatively symmetric about the peak temperature and that both heating and cooling rates were rather slow. Average cooling rates near peak temperature were on the order of 5 to 10°C/s (9 to 18°F/s). It is often convenient to characterize cooling rates according to the time for cooling between 800°C and 500°C (Δt_{8-5}) (1472°F to 932°F) (Ref. 32). Assuming cooling rates of the same order of magnitude throughout the rest of the weld region, as suggested by calculations for arc welds by Adams (Ref. 33), the Δt_{8-5} for these welds was around 50 to 60 s across the entire weld region.

Thermocouples attached to the circumference of the tool at 0.25 and 0.38 in. (6.35 and 9.65 mm) above the shoulder read peak temperatures of 985°C (1805°F) and 930°C (1706°F), respectively — Fig. 2B. The tool temperatures rose during the 180-second plunging period and reached steady state soon after the welding period was begun. Note that the temperature plots for the tool were truncated after a short length since the thermocouples were severed by motion of the flashing. Fortunately, the tool temperature reached steady state before the thermocouples were lost, thus allowing calibration of the emissivity and monitoring of temperature throughout the rest of the weld with the infrared system.

Thermocouple measurements were confirmed by data from the infrared system. Peak surface temperatures of approximately 990°C (1814°F) were measured near the shoulder/workpiece interface using the infrared system. Measurement of temperature at the shoulder/workpiece boundary was not possible during welding since this location was blocked from direct view of the infrared camera by flashing. Consistent with the thermocouple measurements, temperature gradients of 100 to 200°C/cm (540 to 995°F/in.) were determined along the length of the tool with software from the infrared system.

Representative load and torque curves are presented in Fig. 3A and B. The

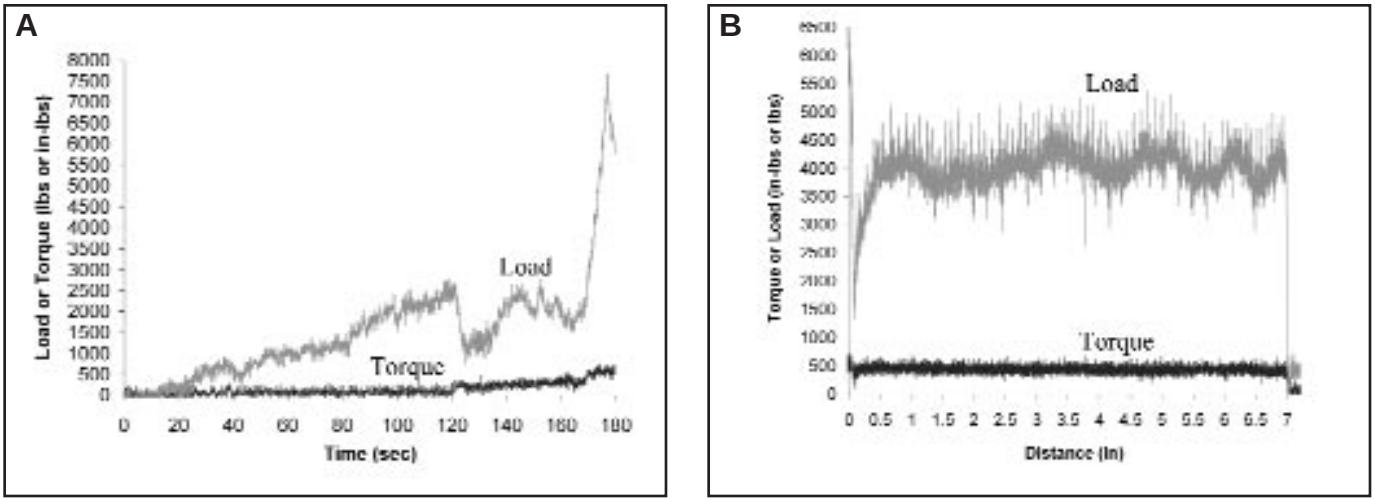

Fig. 3 — A — Load and torque curves during plunge stage for FSW of 1018 steel; B — load and torque curves during weld stage for FSW of 1018 steel.

plunging period lasted almost three minutes — Fig. 3A. During plunging of the tool, the load rose initially when the pin was in contact with the cold workpiece and quickly fell as the material was softened due to heating. The softened material was displaced until the pin again encountered colder material, and the process then repeated. Initial load curves exhibited several "spikes" up to about 2750 pounds of force (lbf) (12.2 kN) during the first two to three minutes of the plunging period prior to welding. The large spike in load up to 7600 lbf (33.8 kN) occurring approximately 175 s into the plunge cycle corresponded to the point in time when the shoulder contacted the top surface of the plate. The torque value rose slowly during the last minute of plunging and reached steady state when shoulder contact occurred.

Average axial loads in the range of 4200 lbf (18.7 kN) were recorded during the welding period for welds made at a travel speed of 1 in./min — Fig. 3B. Average tool pressures calculated using the tool load and shoulder area were approximately 11.5 ksi (79.2 MPa). Note this value is very close to the flow stress reported for mild steel at 1100°C (2012°F) (Refs. 25, 34). Increased tool loads were observed at faster travel speeds. Higher-frequency fluctuations of ±750 lbf (3.3 kN) were observed in the load curve. These rapid fluctuations are similar to those seen by tribologists during friction testing (Ref. 35) and may correspond to discrete stick-slip events that occurred during welding. Low-frequency undulations of ±250 lbf (1.1 kN) were also found. These fluctuations occurred over distances of approximately 1 in. (2.54 cm) and were attributed to the growth and expulsion of flashing around the end of the tool.

Torque on the tool averaged around 500 in.-lb (55 N·m) during the welding period — Fig. 3B. No appreciable change was found in the torque with different travel speeds. The torque curve showed high-frequency variations similar to those of the load curve but none of the low-frequency fluctuations. Fast-Fourier Transform results showed a number of dominant frequencies including those corresponding to the tool rpm and its harmonics, as well as 60-Hz frequencies picked up from nearby electrical equipment. Several other frequencies including those corresponding to the rapid fluctuations mentioned above were also identified. The source of these frequencies is still under investigation. While many of the frequencies are likely spurious, some of them may be related to physical processes occurring during FSW. Identification of these frequencies may lead to further process insight such as those found in machining studies (Refs. 36, 37).

Torque and load values reported here for FSW of mild steel can be compared to those for FSW of other materials, such as Ti and Al alloys (Ref. 38). For example, the average torque for FSW of mild steel was lower than that for FSW of a Ti-6 Al-4 V alloy (675 in.-lb). In addition, it is interesting to note that the load and torque values found for steel were comparable to those determined for FSW of a 7075-T6 Al alloy. However, the steel values were greater than those for FSW of 5083-O, 6082-T6, and 6061-T6 Al alloys.

Comparisons of tool dimensions were made before and after welding using an optical comparator. The metrology data, combined with results of microstructural analysis of the tools and workpiece, suggest changes in tool dimensions stem from both rubbing wear and deformation of the tool. The greatest changes in tool dimensions occurred during the initial plunging stage. Measurements showed the tip of the pin mushroomed similar to a resistance-welding electrode and lost approximately 0.010 in. (0.25 mm) of its original 0.245 in. (6.2 mm) of length during the plunging stage and a total of 0.012 in. (0.30 mm) for the entire weld.

Microstructural Characterization

Features of the base metal microstructure are shown in Fig. 4A and B. The as-received base metal exhibited a microstructure of equiaxed ferrite grains approximately 20 to 30 μm in diameter and smaller grains of fine pearlite, as seen in Fig. 4A. Fig. 4B is an SEM micrograph showing the fine lamellar spacing in a pearlite colony.

A low-magnification optical micrograph of the weld region is presented in Fig. 5. The weld area displayed several microstructurally distinct regions including the stir zone along the weld centerline, the heat-affected zone (HAZ) surrounding the stir zone, and the base metal. Unlike welds on Al alloys, no distinct HDAZ was seen in the steel welds. Note that flow lines and other indications of deformation that persist to room temperature in friction stir welds on Al alloys, such as those found in the HDAZ (Ref. 13), are not found in similar welds on mild steel apparently due to the allotropic transformations experienced during cooling. Hence, the presence of any HDAZ has likely been obscured in the steel welds by these transformations.

EDS results show the light etching features near the bottom center of the stir zone are Mo-enriched regions. Note that the features were not discrete pieces of Mo that broke off from the tool. Rather, they appeared very similar to composite structures

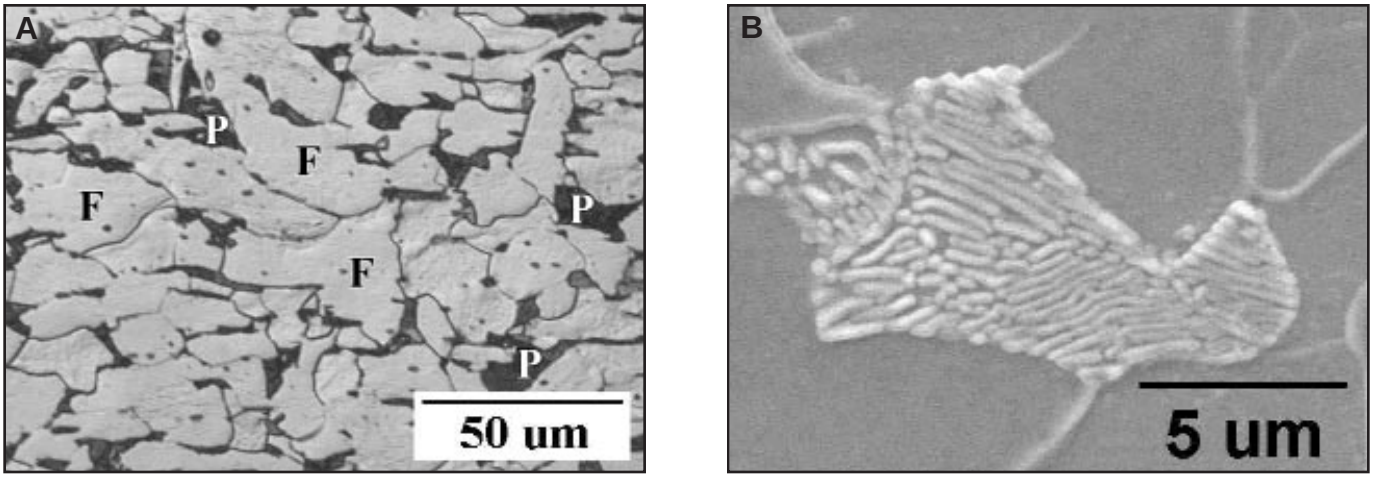

Fig. 4 — Micrographs of the 1018 steel base metal. A — Optical micrograph showing equiaxed grains of ferrite (F) as the major phase and smaller grains of fine pearlite (P) as the minor constituent; B — SEM micrograph showing the fine spacing of the lamellae of the pearlite.

formed in early stages of mechanical alloying during high-energy ball milling (Refs. 39, 40). These features undoubtedly stemmed from transfer and mechanical mixing of tool material with material from the workpiece under high pressures. Comparison of metallographic samples from the weld start area and the remainder of the weld show a greater number of these features in the weld start area, suggesting greater material loss there.

Higher magnification optical micrographs of the weld region are shown in Figs. 6 and 7. Material in the center of the stir zone (Fig. 6A) is essentially hot worked during welding due to interactions with the tool. Microstructural evidence indicates peak temperatures reached well into the austenite phase field, allowing appreciable grain growth. The microstructure of the stir zone was characterized by the presence of ferrite with aligned and nonaligned second phases, grain boundary ferrite, and a ferrite/carbide aggregate that appears to be fine pearlite.

Figure 6B is an optical micrograph of the upper surface of the stir zone. Evidence of considerable microstructural refinement of the top surface can be seen relative to the center of the stir zone. The gradient in microstructural refinement seen here is consistent with the development of a strain gradient as a function of distance from the tool shoulder. Workpiece material closest to the tool shoulder experiences greater amounts of strain relative to material away from the shoulder, resulting in refinement.

As with arc welds (Refs. 41, 42), the microstructures of the different subregions of the HAZ of friction stir welds develop in accord with the local thermal cycle experienced during welding. With increasing distance from the weld centerline, the HAZ exhibited a grain-coarsened region (Fig. 7A) surrounding the stir zone, a grain-refined region (Fig. 7B) encompassing the grain-coarsened region, an intercritical region (Fig. 7C), and a subcritical region containing partially spheroidized carbides and ferrite — Fig. 7D.

Table 2 — Room Temperature Tensile Properties

	Base Metal	Friction Stir Welds[a] (Transverse Orientation)
Yield strength (YS)	45.0 ksi (310 MPa)	48.1 ksi (331 MPa)
Tensile strength (TS)	67.2 ksi (463 MPa)	69.1 ksi (476 MPa)
Elongation to failure	40%	22%
Reduction in area	22%	31%

(a) Failed in base metal.

Mechanical Properties

A plot of the microhardness data as a function of position from the weld centerline is presented in Fig. 8. The hardness of the as-received base metal was approximately 135 VHN. The hardness of the stir zone varied with position ranging from 155 to 175 VHN, depending on the grain size and phases sampled by each indentation. Hardness decreased with increasing distance from the stir zone from approximately 150 to 160 VHN in the grain-coarsened region to between 135 and 140 VHN in the base metal. Despite its smaller grain size relative to the material from the bulk stir zone, the hardness of the microstructurally refined region at the top surface of the stir zone ranged from 155 to 165 VHN.

Samples from properly processed welds passed bend tests to 180 deg (R = 3T or tensile strain at the outer fiber ≈ 15%). Average tensile properties are given in Table 2. Values given in the table indicate the average of at least three tests. Welded samples failed in regions corresponding to the base metal and demonstrated yield and ultimate tensile strengths comparable to those of the base metal. These results suggest the stir zone and HAZ have greater yield and tensile strengths than the base metal. Taken together with the bend ductility, the results indicate acceptable tensile properties for FSW of mild steel.

Discussion

Peak Temperatures and Heat Loss to the Tool

Recall that peak surface temperatures of approximately 1000°C (1832°F) were measured just above the tool shoulder at steady state by both the thermocouples and infrared camera. Additionally, thermal gradients of 100 to 200°C/cm (540 to 995°F/in.) were found along the tool using both methods. As mentioned earlier, determination of the peak temperature at the shoulder/workpiece interface was not possible due to experimental difficulties. Extrapolation of the temperature gradient from the two known positions, assuming steady state and a linear gradient, suggests peak surface temperatures of at least 1100°C (2012°F) at the shoulder and similar temperatures for the workpiece mate-

Fig. 5 — Optical micrograph of a transverse section of a friction stir weld on 1018 steel. The stir zone, HAZ, and base metal regions can be distinguished.

rial in contact with the shoulder.

Microstructural evidence is also consistent with peak temperatures above 1100°C (2012°F) in the workpiece. Bear in mind that a grain-coarsened region was observed in the HAZ immediately adjacent to the stir zone. As discussed in a later section of this paper, formation of a grain-coarsened region in the HAZ of welds in this alloy requires temperatures of at least 1100°C (2012°F). Moreover, temperatures within the stir zone are believed to be greater than those of the HAZ. In fact, extrapolation of the gradients in microstructure in the HAZ to the Fe-Fe_3C phase diagram suggests peak temperatures in the stir zone above 1200°C (2192°F).

Note that knowledge of the thermal gradient along the tool allows approximation of the heat flux lost along the length of the tool using Fourier's Law (Ref. 43) (assuming radiative and convective losses are negligible). Estimates of the flux, using a temperature-compensated thermal conductivity for the tool material and assuming one-dimensional heat flow, are on the order of 100 to 200 W/cm^2 (315 x 10^3 to 630 x 10^3 Btu/h•ft^2). The magnitude of the heat flux lost to the tool is useful in establishing boundary conditions for modeling of heat flow during FSW.

In addition, the power dissipated in heating the tool can be estimated (assuming a uniform flux) as the product of flux and the cross-sectional area of the tool. These calculations suggest the power absorbed by the tool ranged from 300 to 600 W (1.025 x 10^3 to 2.050 x 10^3 Btu/h) for FSW of mild steel during steady state.

It is also important to note that torque and weld rpm data also permit estimation of total weld power and heat input for FSW. Comparisons can then be made with other welding processes such as gas metal arc welding (GMAW). Once the total power and power lost to the tool are known, the process efficiency can be approximated. Initial estimates suggest a process efficiency of approximately 0.75 for the conditions described in this paper. Further details of calculations of power and heat input for FSW of mild steel, comparisons with estimated GMAW values, and estimations of process efficiency for FSW of steel will be discussed in a subsequent paper by the authors.

Microstructural Evolution in the HAZ

With the possible exception of an HDAZ, the HAZ experiences little or no deformation during FSW and consequently is similar to the HAZ found in arc welds. Hence, microstructural evolution in the various regions of the HAZ of friction stir welds on 1018 steel alloys can be approximated with the aid of a section of the Fe-Fe_3C phase diagram shown in Fig. 9. The vertical line in the phase diagram indicates the composition of a 0.18 wt-% C alloy. Note that use of a binary phase diagram to model transformation behavior in a multicomponent alloy such as 1018 introduces some uncertainties with respect to the position of phase boundaries. Moreover, use of the equilibrium diagram does not capture the time-dependent nature of transformations experienced during FSW. Hence, Fig. 9 serves only to illustrate schematically the effective peak temperatures experienced in the different regions of the HAZ.

As shown in Fig. 9, the microstructures of the regions of the HAZ can be spatially correlated to peak temperatures on the phase diagram, with effective peak temperatures decreasing with distance from the stir zone. Material in the grain-coarsened region experienced the highest temperatures in the HAZ. The HDAZ, if it ever existed, was likely contained within the area that became the grain-coarsened region. Microstructural and experimental evidence suggest peak temperatures were well above the effective A_3 temperature for this alloy during welding, thus allowing some austenite grain growth. Evidence for the existence of a HDAZ was probably lost during decomposition of the austenite grains on cooling. The grain-coarsened region contained phases similar to those of the stir zone but somewhat smaller in scale due to the lower peak temperatures.

Microstructural results indicate peak temperatures encountered in the grain-refined region fell just above the effective A_3 temperature. The decomposition of austenite to ferrite and pearlite on cooling promoted a finer grain size in this region. The microstructure of this region contained fine grains of pearlite and proeutectoid ferrite.

The intercritical region was characterized by a bimodal distribution of ferrite grain sizes. Material in the intercritical region was exposed to peak temperatures in the two-phase (ferrite and austenite) region between the effective A_1 and A_3 temperatures. This thermal cycle caused transformation of the pearlite to austenite on heating (with the reverse reaction on cooling) and resulted in refinement of the pearlite colonies and some of the ferrite

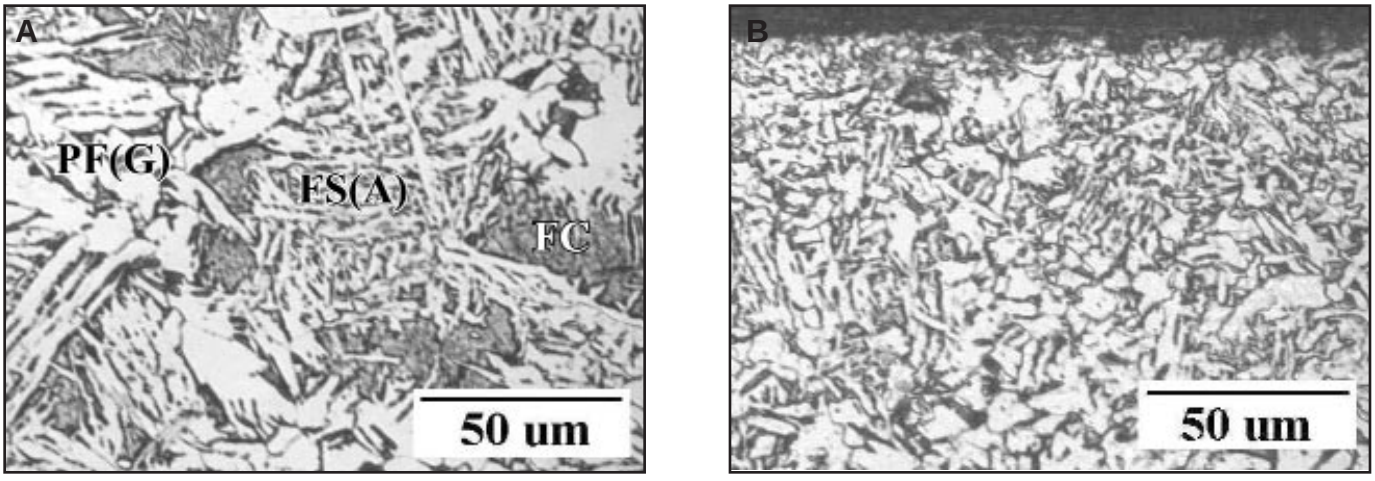

Fig. 6 — Optical micrographs of the stir zone. A — Center of stir zone: grain boundary ferrite [PF(G)], ferrite-carbide aggregate [FC], and ferrite with aligned second phase [FS(A)]; B — top surface of stir zone: finer ferrite.

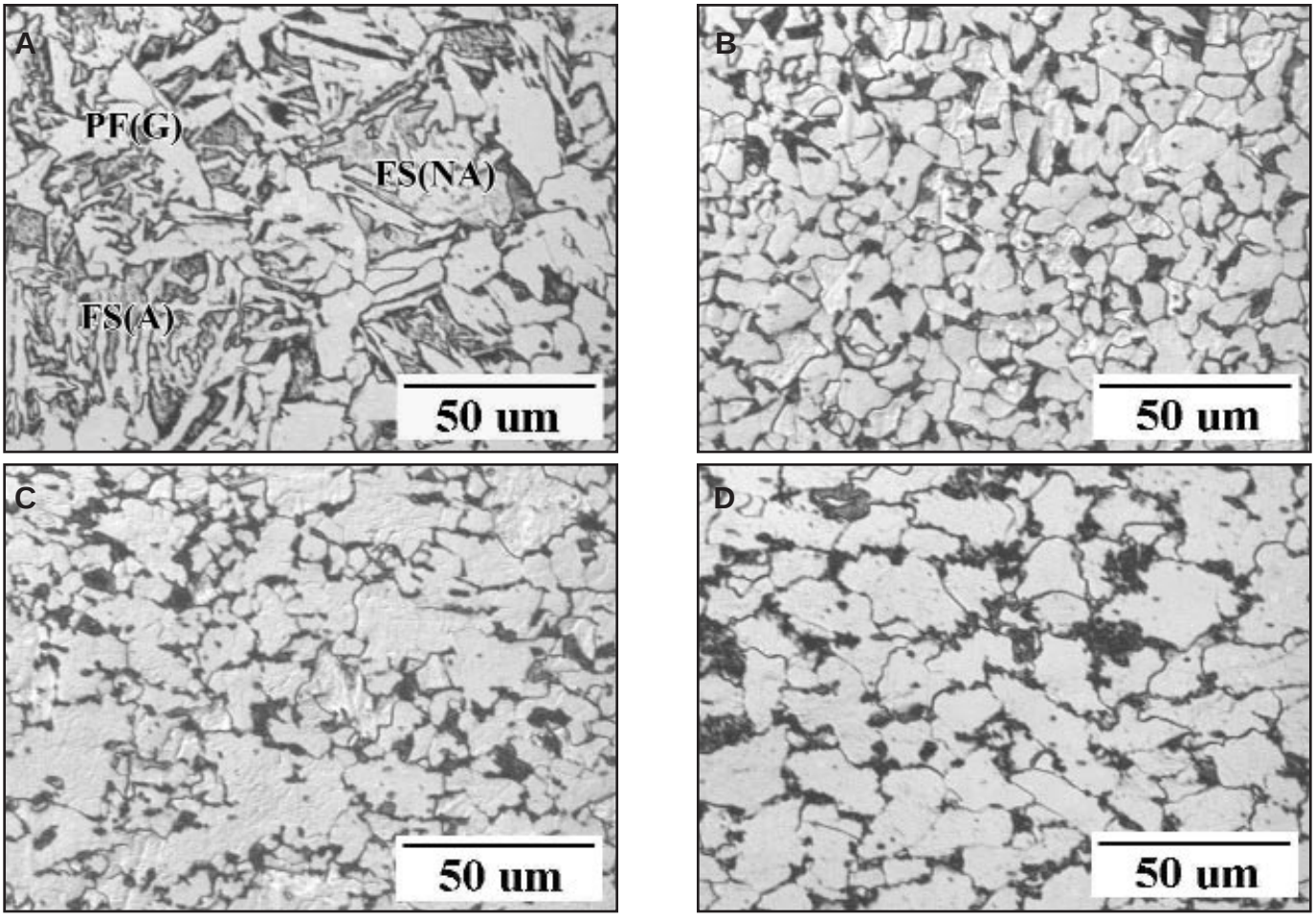

Fig. 7 — Optical micrographs of the different regions of the HAZ. A — Grain-coarsened region: grain boundary ferrite [PF(G)] and ferrite with aligned [FS(A)] and nonaligned second phases [FS(NA)]; B — grain-refined region: pearlite (black) and proeutectoid ferrite (white); C — intercritical region: pearlite (black) and ferrite (white); D — spheroidized carbide region: pearlite (black) and ferrite (white).

grains (Ref. 40). Microstructural observations imply the material in the region of spheroidized carbides experienced sufficient time below the A_1 temperature to allow partial homogenization and spheroidization of the cementite.

The large microstructural features of the grain-coarsened HAZ and the presence of pearlite in the grain-refined region attest to the slow cooling rates estimated for the HAZ. In fact, the microstructures of the grain-coarsened and grain-refined regions are consistent with those predicted by the continuous-cooling transformation diagram developed for arc welds on a similar steel (Ref. 44). In agreement with the observed microstructures and cooling rates, the diagram predicts the presence of mainly ferrite and pearlite with some intermediate product for a Δt_{8-5} of 60 s, such as that experienced in this work.

Microstructural Evolution in the Stir Zone

Microstructural evolution in the stir zone is not as easy to interpret as that in the HAZ. While the HAZ experiences a thermal cycle only, the stir zone (and any HDAZ) experiences both thermal and mechanical cycles. Hence, effects of the combined thermomechanical cycle must be considered in a discussion of microstructural development of the stir zone.

The thermomechanical cycle of the stir zone of mild steel involves hot working processes. As discussed earlier, the important parameters that control microstructural evolution are the total strain, the strain rate, and the temperature cycles. Temperature measurements and microstructural evidence indicate peak temperatures in the stir zone exceed 1100°C (2012°F). At 1100°C (2012°F), the mild steel is austenitic (FCC). Total strains during FSW are thought to exceed 10^0 (=1), and strain rates have been estimated at 10^2 s^{-1} (Ref. 7).

Several restorative processes may operate solely or in combination during hot working including dynamic recovery, dynamic recrystallization, and metadynamic recrystallization (Ref. 25). Dynamic recrystallization may also be defined as occurring discontinuously (nucleation of new grains and growth by motion of high-angle grain boundaries) or continuously (increasing misorientation of existing subgrain boundaries due to absorption of dislocations, also described as extended recovery) (Ref. 45). The operative mechanism is dependent on the stress (or strain) and strain rate histories, as well as the stacking fault energy (SFE) of the material (Ref. 25). For a given material, higher stresses (or strains) and strain rates tend to promote discontinuous recrystallization. Moreover, materials with low SFE, such as mild steels in the austenitic phase field, generally undergo discontinuous dynamic recrystallization since the dislocations tend to dissociate making recovery (involving cross-slip and climb mechanisms) more difficult. Al alloys, with their high SFE, however, tend to undergo continuous dynamic recrystallization (Ref. 22).

Under the conditions of FSW encountered in this work (T>1100°C and $\dot{\varepsilon} \approx 10^2 s^{-1}$), the material in the stir zone of mild steel is expected to undergo discontinuous dynamic recrystallization (Refs.

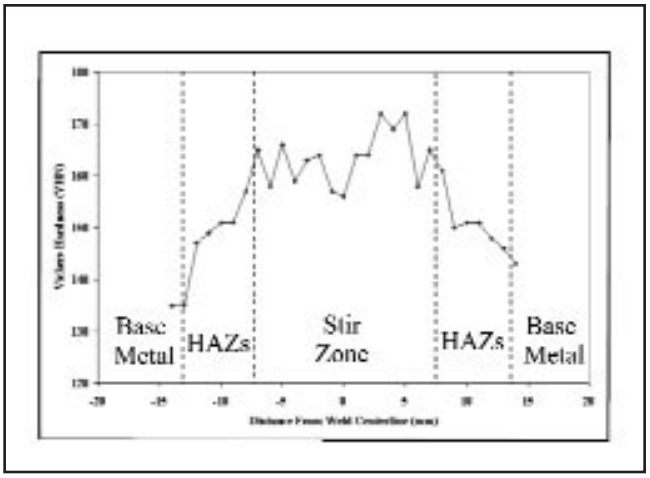

Fig. 8 — Microhardness traverse for friction stir welded 1018 mild steel. Hardness readings are spatially correlated to the different regions of the weld.

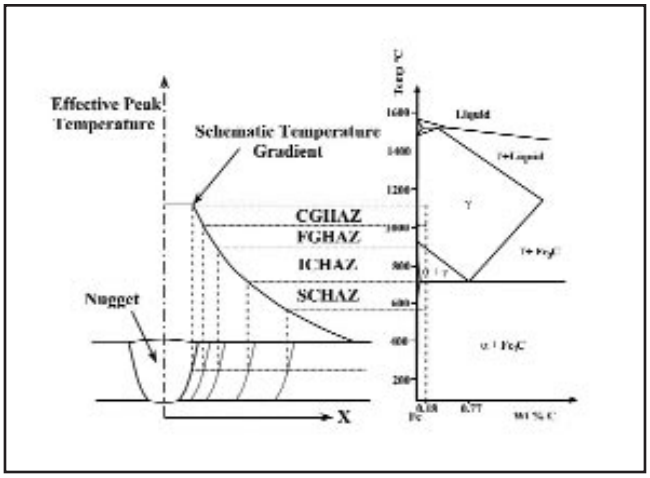

Fig. 9 — Schematic illustration of the different regions of the HAZ of a friction stir weld on mild steel and their relation to effective temperatures in the Fe-Fe_3C binary system.

25, 34), especially in the region near the tool shoulder, which experiences greater and more prolonged strain relative to the rest of the stir zone. Consistent with the principles of recrystallization (Ref. 46), the greater strain near the surface gives rise to a finer recrystallized grain size. However, the slow cooling rates experienced in the stir zone after passage of the tool are also expected to allow considerable time at temperature for grain growth to occur throughout the remainder of the stir zone, thereby yielding the coarser microstructures observed away from the top surface.

Tool Life Issues

As discussed earlier, wear and deformation of the tool, especially the pin, occurs during FSW of mild steel using current tool materials. While the wear and deformation of the tool do not appear to impact tensile properties greatly, there is considerable concern regarding tool life. In fact, further advances in FSW of high-temperature materials such as steels, Ti alloys, and Ni alloys rely on finding tool materials, tool designs, and processing strategies to extend tool life.

In this work, the greatest amount of wear and deformation was found to occur during the plunging stage. This phenomenon likely occurs due to the high load spikes during plunging that evidently derive from the greater flow stress of the cold workpiece material. Strategies involving preheating the plunge area and maintaining slow plunge rates, as well as use of a partial-penetration, partial-diameter hole, act to limit wear and deformation during plunging. Moreover, an oversize pin can be utilized to allow for material loss during plunging, yielding a proper sized pin for the welding stage. However, these strategies do not completely resolve the problems, and more work is needed in this area.

Criteria for selection of new materials and designs are clearly needed. Of course, the ideal tool material should be stronger and harder than the workpiece material at welding temperatures. However, other requirements for successful tool materials are not well understood. For example, the effects of the relationships between the thermophysical properties of the tool and the workpiece on heat flow and tool life must be studied. Furthermore, the metallurgical compatibility between the tool and workpiece, and subsequent effects on tool life, must be better understood. For instance, tool/workpiece alloy combinations that form solid solutions may promote alloying of the surface of the tool and subsequent local changes in tool properties that cause a type of high-temperature corrosive wear to occur.

Conclusions

1) Defect-free welds were produced on of 0.25-in.-thick (6.35-mm) mild steel with FSW over a range of travel speeds from 1 to 4 in./min (0.42 to 1.68 mm/s). Tool loads during FSW of mild steel at 1 in./min (0.42 mm/s) were approximately 4200 lbf (18.7 kN), while measured torques were in the range of 500 in.-lb (55 N·m).

2) Peak surface temperatures close to 1000°C (1832°F) were measured on the tool above the shoulder during FSW using thermocouples and an infrared camera system. Extrapolation of measured temperatures and microstructural evidence suggest peak temperatures of the stir zone exceeded 1100°C (2012°F) and likely surpassed 1200°C (2192°F).

3) Comparisons before and after welding combining both metallographic and metrology techniques suggest changes in tool dimensions resulted from both rubbing wear and deformation of the tool. The greatest changes in tool dimensions occurred during the initial plunging stage.

4) The weld region displayed several microstructurally distinct regions including the stir zone (along the weld centerline), a grain-coarsened region (surrounding the stir zone), a grain-refined region (encompassing the grain-coarsened region), an intercritical region, and a subcritical region containing partially spheroidized carbides. The different regions develop in accord with the local thermomechanical cycle.

5) Welded samples failed in regions corresponding to the base metal and demonstrated yield and ultimate tensile strengths comparable to those of the base metal. Welded samples passed bend tests to 15% strain in the outer fiber.

6) Results of this study have demonstrated the feasibility of FSW of steel without loss of tensile properties. Based on these results, FSW of transformation-hardenable steels, HSLA steels, and stainless steels may be feasible.

Acknowledgments

The authors wish to thank D. S. LaPolla and B. Sikora of EWI for their assistance in this work. The authors also extend their appreciation to Dr. M. Q. Johnson and Dr. J. E. Gould, both of EWI, for their careful reviews of this manuscript and for helpful discussions throughout the course of this work. Finally, the authors wish to acknowledge the support of the EWI Cooperative Research Program (CRP) in funding this effort.

References

1. Thomas, W. M., et al. 1991. International Patent Application No. PCT/GB92/02203 and GB Application No. 9125978.8.

2. Gould, J. E. , Feng, Z., and Ditzel, P. 1996. Preliminary modeling of the friction stir weld-

ing process. *Proceedings of ICAWT*, pp. 297–310. EWI, Columbus, Ohio.

3. Kong, H. S., and Ashby, M. F. 1991. Friction heating maps and their applications. *MRS Bulletin* 16(10): 41–48.

4. Feng, Z., Gould, J. E., and Lienert, T. J. 1998. A heat flow model for friction stir welding of aluminum alloys. *Proceedings of Hot Deformation of Aluminum Alloys*. pp. 149–158. TMS.

5. Gao, Y., and Wagoner, R. H. 1987. A simplified model for heat generation during the uniaxial tensile test. *Metallurgical Transactions* 18A: 1001–1009.

6. Braga, H. C., and Barbosa, R. A. 1992. Simulation of the increase in temperature due to adiabatic heating in hot deformation processes. *Proceedings of 47th Brazilian Association of Metallurgy and Materials (ABM) Annual Conference* pp. 441–457. ABM.

7. Nunes, A. C., Jr., Bernstein, E. L., and McClure, J. C. 2000. A rotating plug model for friction stir welding. Submitted for publication in the *Welding Journal*.

8. Murr, L. E., Liu, G., and McClure, J. C. 1997. Dynamic recrystallization in friction stir welding of aluminum alloy 1100. *Journal of Materials Science* 16: 1801–1803.

9. Christner, B. K., and Sylva, G. D. 1996. Friction stir weld development for aerospace applications. *Proceedings of ICAWT 1996*, pp. 311–320. EWI, Columbus, Ohio.

10. Li, Z. X., Arbegast, W. J., and Hartley, P. J. 1998. Microstructure characterization and stress corrosion evaluation of friction stir welded Al 2195 and Al 2219 alloys. *Proceedings of the Fifth International Conference on Trends in Welding Research*, pp. 568–573. Materials Park, Ohio: ASM International.

11. Strangwood, M., Berry, J. E., Cleugh, D. P., Leonard, A. J., and Threadgill, P. L. 1999. Characterization of the thermo-mechanical effects on microstructural development in friction stir welded age hardening aluminium-based alloys. *Proceedings of the First International Conference on Friction Stir Welding*. Session 11, Paper 3. Cambridge, England: TWI.

12. Reynolds, A. P. 1998. Mechanical and corrosion performance of GTA and friction stir welded aluminum for tailor welded blanks: alloys 5454 and 6061. *Proceedings of the Fifth International Conference on Trends in Welding Research*, pp. 563–567. Materials Park, Ohio: ASM International.

13. Karlsson, L., Svensson, L.-E., and Larsson, H. 1998. Characteristics of friction stir welded aluminum alloys. *Proceedings of the Fifth International Conference on Trends in Welding Research*. pp. 574–579. Materials Park, Ohio: ASM International.

14. Haagensen, P. J., Midling, O. T., and Ranes, M. 1995. Fatigue performance of friction stir butt welds in a 6000 series aluminum alloy. *Proceedings of the International Conference on Computer Methods and Experimental Methods for Surface Treatment Effects II,* pp. 225–237. Computational Mechanics Publications.

15. Lienert, T. J., Grylls, R. J., Gould, J. E., and Fraser, H. L. 1998. Deformation microstructures in friction stir welds on 6061-T651. *Proceedings of Hot Deformation of Aluminum Alloys,* pp. 159–167. TMS.

16. Murr, L. E., Liu, G., and McClure, J. C. 1998. A TEM study of precipitation and related microstructures in friction stir welded 6061 aluminum. *Journal of Materials Science* 33: 1243–1251.

17. Sato, Y. S., Kokawa, H., Enomoto, M., and Jogan, S. 1999. Microstructural evolution of 6063 during friction stir welding. *Metallurgical and Materials Transactions* 30A: 2429–2437.

18. Rhodes, C. G., Mahoney, M. W., Bingel, W. H., Spurling, R. A., and Bampton, C. C., 1997. Effects of friction stir welding on microstructure of 7075 aluminum. *Scripta Materiala* 36(1): 69–75.

19. Mahoney, M. W., Rhodes, C. G., Flintoff, J. G., Bingel, W. H., and Spurling, R. A. 1998. Properties of friction stir welded 7075 T651 aluminum. *Metallurgical and Materials Transactions* 29A: 1955–1964.

20. Jata, K. V., Sankaran, K. K., and Ruschau, J. J. 2000. Friction-stir welding effects on microstructure and fatigue of aluminum alloy 7050-T7451. *Metallurgical and Materials Transactions* 31A: 2181–2192.

21. Kinchen, D. G., Li, Z., and Adams, G. P. 1999. Mechanical properties of friction stir welds in Al-Li 2195-T8. *Proceedings of the First International Conference on Friction Stir Welding.* Session 9, Paper 2. Cambridge, England:TWI.

22. Jata, K. V., and Semiatin, S. L. 2000. Continuous dynamic recrystallization during friction stir welding of high-strength aluminum alloys. *Scripta Materiala* 43: 743–749.

23. Dawes, C. J., and Thomas, W. M. 1996. Friction stir process welds aluminum alloys. *Welding Journal* 75 (3): 41–45.

24. Wang, X. L., Feng, Z., David, S. A., Spooner, S., and Hubbard, C. R. 2000. Neutron diffraction study of residual stresses in friction stir welds. Submitted for publication in *Proceedings of The International Conference on Residual Stresses-6.*

25. Courtney, T. H. 1990. *Mechanical Behavior of Materials.* pp. 309–317. New York. N.Y.: McGraw-Hill.

26. *EWI Insights*. Vol. 11, no. 4, 1998.

27. Lienert, T. J., and Gould, J. E. 1999. Friction stir welding of mild steel. *Proceedings of the First International Conference on Friction Stir Welding.* Session 10, Paper 3. Cambridge England: TWI.

28. Thomas, W. M.,Threadgill, P. L. , and Nicholas, E. D. 1999. Feasibility of friction stir welding of steel. *Science and Technology of Welding and Joining* 4(6): 365–372.

29. Occupational Safety and Health Administration, 2001. *Occupational Exposure to Hexavalent Chromium*. OSHA RIN: 1218-AB45.

30. IIW Document IX-1533-88 IXJ-123-87 Revision 2, 1998. *Guide to the Light Microscope Examination of Ferritic Steel Weld Metals*. IIW.

31. ASTM, 2000. ASTM Standard E 8-00: Standard test methods for tension testing of metallic materials. *Annual Book of ASTM Standards*. Vol. 03.01.

32. Easterling, K. 1983. *Introduction to the Physical Metallurgy of Welding*. pp. 23–26. London, U.K.: Butterworths & Co.

33. Adams, C. M. 1958. Cooling rates and peak temperatures in fusion welding. *Welding Journal* 37(5): 210-s to 215-s.

34. Hughes, K. E., Nair, K. D., and Sellars, C. M. 1974. Temperature and flow stress during hot extrusion of steel. *Metals Technology* 1(4): 161–169.

35. *ASM Handbook*, Vol. 18, Friction, lubrication and wear technology, p. 48. Materials Park, Ohio: ASM International.

36. M. N. Hamdan and A. E. Bayoumi, 1989. An approach to study the effects of tool geometry on the primary chatter vibration in orthogonal cutting. *Journal of Sound and Vibration* 128(3): 451–469.

37. Bayoumi, A. E., Barnwal, S., and Hutton, D. V. 1993. Prediction of flank wear and engagements from force measurements in end milling operations. *Wear* 170: 255–266.

38. Lienert, T. J., and Stellwag, W. L., Jr. 2001. Determination of load, torque, and tool temperature during friction stir welding of aluminum alloys. *Abstracts of Papers* from the 2001 AWS Convention, pp. 152–155. Miami, Fla: American Welding Society.

39. Benjamin, J. S., and Volin, T. E. 1974. The mechanism of mechanical alloying. *Met. Trans.* 5A: 1929–1934.

40. Benjamin, J. S. 1976. Mechanical alloying. *Scientific American* 234(5): 40–48.

41. Easterling, K. 1983. *Introduction to the Physical Metallurgy of Welding*. pp. 141–143. London, U.K.: Butterworths & Co.

42. Kuo, S. 1987. *Welding Metallurgy*. pp. 326–329.New York, N.Y.: John Wiley and Sons.

43. Holman, J. P. 1976. *Heat Transfer*. pp. 1–11. New York, N.Y.: McGraw-Hill.

44. Linnert, G. E. 1967. *Welding Metallurgy: Carbon and Alloy Steels*. 3rd ed., Vol. 2. pp. 312–325. Miami, Fla: American Welding Society. — Excerpted from M. Inagaki and H. Sekiguchi, 1960. Continuous cooling transformation diagrams of steels for welding and their applications. *Transactions of the National Research Institute for Metals* (Japan) 2(2): 102–125.

45. Humphries, F. J. 1997. A unified theory of recovery, recrystallization and grain growth based on the stability and growth of cellular microstructures. *Acta Materiala* 45(10): 4231–4240.

46. Shewmon, P. G. 1969. *Transformations in Metals.* 1st ed. pp. 93–97, New York, N.Y.: McGraw-Hill.